Mine Water and the Environment (2019) 38:391–401
https://doi.org/10.1007/s10230-019-00590-9

TECHNICAL ARTICLE

Magnetic Flocculation Treatment of Coal Mine Water and a Comparison of Water Quality Prediction Algorithms

Xiaohang Zhang[1] · Xuwen He[1] · Ming Wei[2] · Fuqin Li[3] · Pin Hou[1] · Chunhui Zhang[1]

Received: 23 November 2017 / Accepted: 11 January 2019 / Published online: 19 January 2019

Abstract

In this study, laboratory-scale magnetic flocculation systems were set up and the optimal coagulant and flocculent dosage, magnetic seed immersion, pH, stirring intensity, and precipitation time were all evaluated. A total of 729 expansion reaction conditions were generated, and 700 of the expansion reaction conditions were used to train a back-propagation neural network (BPNN) and general regression neural network (GRNN). The other 29 conditions were used to verify the networks' regression ability. The optimum coagulant was poly-aluminum chloride at a dosage of 100 mg/L; the optimum flocculent was anionic polyacrylamide at a dosage of 4 mg/L; the optimum size of the magnetic seed was 200 mesh at a dosage of 1 g/L; and the optimum stirring intensities were 300 r/min for the coagulation tank, 200 r/min for the mixing tank, and 100 r/min for the flocculation tank. Comparing BPNN and GRNN, the GRNN's regression performance better matched the relationship between the reaction conditions and results.

Keywords Magnetic seed · Back-propagation neural network · General Regression Neural Network · Regression ability

Introduction

In underground coal mining, a large amount of mine water will often be pumped to the surface. In general, this water contains high concentrations of suspended solids (SS) and a variety of other potentially hazardous materials. The direct discharge of these waters will pollute the mining area's environment and aggravate water supply difficulties in arid or semi-arid areas, and in cities that require large amounts of water (Gao et al. 2013; Kirby et al. 2014, 2015; Wang et al. 2014). Also, if the water is discharged directly without treatment, the SS can cause soil sealing and the other hazardous materials can contaminate the soil. In water treatment, removing the SS is always the key first step. If SS removal is not sufficiently effective, subsequent treatment steps are rendered less effective. Therefore, an efficient SS removal technique is essential to coal mine water reutilization.

Magnetic flocculation is a new technology (Zhao et al. 2015) that has the advantages of high separation efficiency and low operating costs. The process enhances collision efficiency and frequency of colloidal particles and causes colloidal particles to aggregate into larger flocs due to the decreased colloidal stability (Yiacoumi et al. 1996). Therefore, magnetic flocculation has a wide range of applications for removal of suspended solids (Li et al. 2010; Tsouris and Scott 1995; Yiacoumi et al. 1996).

Mathematical models are essential tools to assure proper operation and better control of wastewater treatment plants (Guclu and Dursun 2010). However, the characteristics of the wastewater treatment process dictate that conventional mathematical models that assume relatively simple relationships between the variables are not applicable. Compared with conventional mathematical approaches, an artificial neural network (ANN) has a stronger ability to build accurate non-linear regression relationships between variables of

Electronic supplementary material The online version of this article (https://doi.org/10.1007/s10230-019-00590-9) contains supplementary material, which is available to authorized users.

✉ Xuwen He
hexuwen@sina.com.cn

[1] School of Chemical & Environmental Engineering, China University of Mining & Technology (Beijing), Xueyuan Rd, Haidian District, Beijing 100083, China

[2] Party Committee, Hebei Vocational College of Politics and Law, 569 North Friendship Street, Xinhua District, Shijiazhuang City 050061, Hebei Province, China

[3] Hebei University of Engineering, 199 Guangming nan Str, Hanshan District, Handan City 056038, Hebei Province, China

a complex system. ANN is usually used for biological processes (Almeida 2002; Hong et al. 2007; Pendashteh et al. 2011), but there is no report of it being used to investigate magnetic flocculation. We set up an experimental apparatus and monitored water turbidity and SS removal rates to determine the optimal conditions. To obtain more quality data to train the ANN, the experimental conditions were adjusted within a narrow range of the optimum, and then the recorded data were used to train a back-propagation neural network (BPNN) and general regression neural network (GRNN). The regression performance of both ANNs was then compared statistically.

Materials and methods

Raw water source

The coal mine water used in this research came from a mine in southern Hebei, China. Its water quality is presented in Table 1. A zeta potentiometer (Zetasizernano zs90, Malvern Instruments, Westborough, MA, USA) was used for zeta potential analysis. A particle size analyzer (Mastersizer 2000, Malvern) was used for particle size analysis (Fig. 1). The experiment was conducted in a mine water treatment laboratory where the raw water could be transported to the experimental apparatus via a submersible pump in a mine water pool.

Table 1 Water qualities index of the coal mine water

Turbidity/(NTU)	COD/(mg/L)	SS/(mg/L)	Oil/(mg/L)	pH	Zeta potential/(mV)
49–86	156–238	219–575	3.4583–3.7564	7.2–7.9	− 13.833

COD chemical oxygen demand, *SS* suspended solid

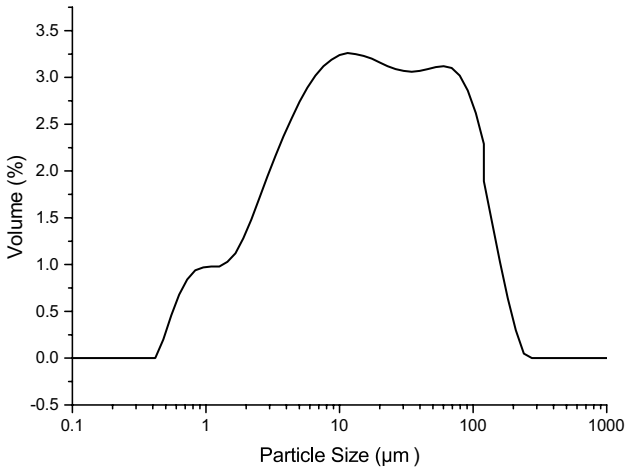

Fig. 1 The particle size distribution of coal mine water

Materials

Three different types of coagulant commonly used in generic water treatment plants were tested in this experiment: poly-aluminum chloride (PAC), ferric chloride ($FeCl_3$), and aluminum sulfate ($Al_2(SO_4)_3$). The concentration of each aqueous solution was 1%. The PAC ($\left[Al_m(OH)_n(H_2O)_x\right] \cdot Cl_{3m-n}(n \le 3m)$, solid (density = 0.48–0.60 g/cm^3; 28% Al_2O_3; ≤ 0.2% of insoluble substances) was provided by Jinchen Co. Ltd., Henan, China). The $FeCl_3$ (solid (density = 1.43 g/cm^3; > 40% $FeCl_3$; ≤ 0.25% $FeCl_2$; ≤ 0.3% of insoluble substances) was provided by Luonier Biotech Co. Ltd., Hebei, China). The aluminum sulfate, $Al_2(SO_4)_3 \cdot 14H_2O$ (density = 1.32–1.33; 8.3% Al_2O_3; < 0.07% of insoluble substances), was provided by Miaosen Environmental Protection Technology Co. Ltd., Henan, China.

Three different flocculants were also studied: cationic, anionic, and non-ionic polyacrylamide (PAM). Solid (density = 1.30 g/cm^3, 12 million of molecular weights; provided by Jinchen water treatment materials Co., Ltd, Henan, China). Again, the concentration of the aqueous solution was 1‰.

The mesh size of the magnetic seed (Fe_3O_4) also influences the turbidity removal rate (TRR) and SS removal rate (SRR). A 200-mesh and a 300-mesh magnetic seed were tested. Solid (density = 5.15 g/cm^3; provided by Ma'anshan Tiangong Technology Co. Ltd., Anhui, China).

Experimental apparatus and monitoring system

Laboratory-scale magnetic flocculation systems were set up as continuous-flow reactors in this experiment. Figure 2 shows the schematic diagram of the magnetic flocculation systems, including an equalization tank, a clean water tank, a treatment sub-system, and a monitoring sub-system. Both the equalization and clean water tank volumes were 30 L. The treatment sub-system was composed of a coagulation tank, a mixing tank, a sedimentation tank, stirring blades, a pressurized pipeline centrifugal pump (WILO/PB-H089EAH, Germany), a pneumatic diaphragm pump (Ingersoll Rand/QBY-10, England, to pump the mud at the bottom of the sedimentation tank), and a hydro-cyclone (WKD/FX-10, China), which was connected with the outlet of the mud pump. The monitoring sub-system was composed of an on-line turbidity meter composed of a sensor (HACH/ULTRATURB plus SC, USA) and a controller (HACH/SC1000, USA), an on-line thermometer (SHIAO/SA10RS485, China), a frequency converter (SERPSON, China), which was used to control the rotation speed of

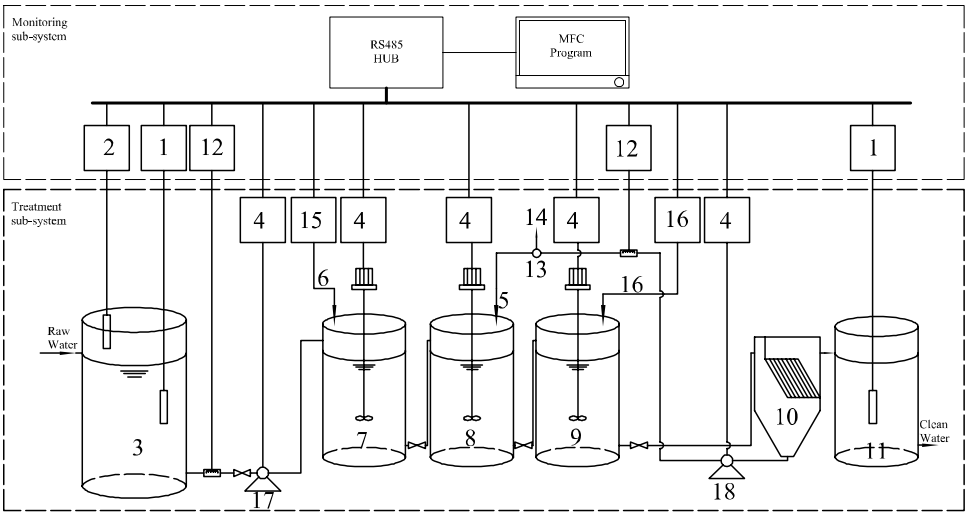

Fig. 2 Schematic diagram of the magnetic flocculation systems in this experiment

1-Turbidity Meter
2-Thermometer
3-Equalization Tank
4-Frequency Converter
5-Magnetic Seed
6-Coagulant
7-Coagulation Tank
8-Mixed Tank
9-Flocculation Tank
10-Sedimentation Tank
11-Clean Water Tank
12-Electromagnetic Flowmeter
13-Hydrocyclone
14-Waste Residue
15-Coagulant Dosing Apparatus
16-Flocculant Dosing Apparatus
17-Pressurized Pump
18-Mud Pump

each motor, a coagulant dosing apparatus, flocculent dosing apparatus, and the MFC program in the computer. All of the monitoring data were transferred to the MFC program in the computer via a RS485 interface, and based on the monitoring data, the program controlled the various mechanisms in the magnetic flocculation systems via the same interface. The magnetic seed that we used came from magnetite ore and was smoothed by a ball crusher.

Experimental methods

Referring to Fig. 2, the raw water was pumped by the pump (17) into the coagulation tank (7). Coagulant (6) was injected into the coagulation tank by the dosing apparatus (15). The coagulation tank outlet flowed into the mixing tank (8), and the magnetic seed (5) was re-injected into the mixing tank by the hydro-cyclone (13). The mixing tank outlet flowed into the flocculation tank (9). Flocculent (16) was injected into the flocculation tank by the dosing apparatus (16). The flocculation tank outlet flowed into the sedimentation tank (10) under gravity, and the flocs generated by coagulation were separated from the water. The clean water with no flocs flowed into the clean water tank (11) from the overflow weir set at the upper part of the sedimentation tank, while the relatively heavy magnetic flocs were deposited at the bottom of the sedimentation tank, and the sediment was reinjected into the mixing tank though the hydro-cyclone. In the hydro-cyclone, the flocs that adhered to the magnetic seed were peeled off by the power of centrifugal force, radial buoyancy, and fluid force. The magnetic seed, with its higher density, drained from the bottom of the hydro-cyclone to finally be reinjected into the mixing tank. The flocs that were removed from the magnetic seed and the water drained from the overflow port of the hydro-cyclone.

The coagulation, mixing, and flocculation tanks were equipped with stirring blades that were driven by the rotation of the motor, and the rotation speed was adjusted by the frequency converter (4). The raw wastewater tank was equipped with an on-line turbidity meter (1) and an on-line thermometer (2). The clean water tank was also equipped with an on-line turbidity meter. The inlet flow was controlled by the pipeline centrifugal pump (17) and the magnetic seed flow rate was adjusted by the mud pump (18), and both pump speeds were adjusted by a frequency converter. The on-line turbidity meter, on-line thermometer, frequency converter, coagulant dosing apparatus, flocculent dosing apparatus, and electromagnetic flow meter were connected to the computer via the RS485 interface. The monitoring and control software installed on the computer side was the self-developed MFC program—magnetic flocculation integrated control system (MFICS). Its function was to change the experimental conditions in an unattended method and save the monitoring data automatically. The application architecture is shown in Fig. 3; the

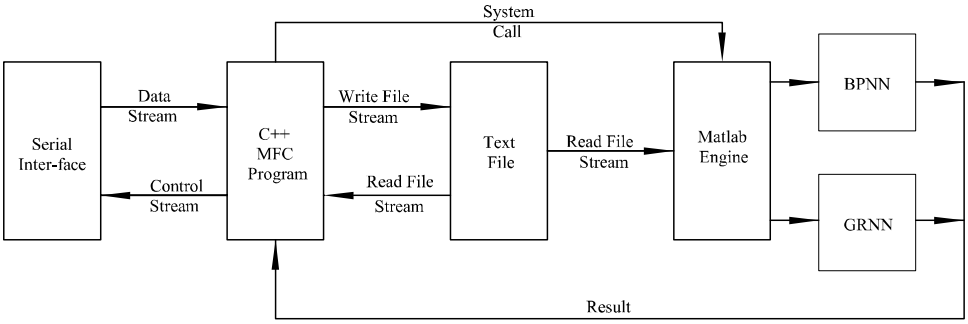

Fig. 3 Application architecture of the magnetic flocculation integrated control system

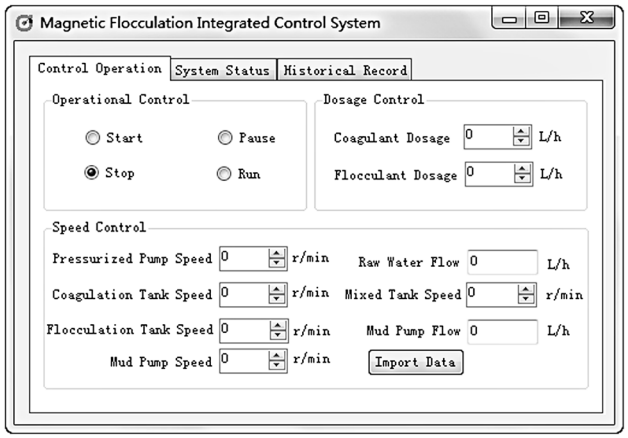

Fig. 4 Magnetic flocculation integrated control system user-interface

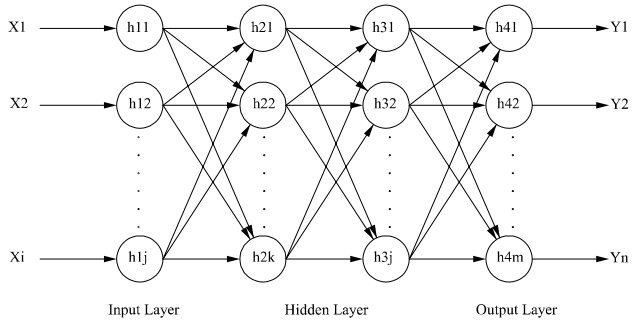

Fig. 5 Typical structure of BPNN

program user interface is shown in Fig. 4. The program had three modules: control operation, system status, and historical record. The control operation module was used to change the actuating mechanism's frequency and speed. The system status module displayed the system's running parameters and monitored data, such as water temperature and turbidity. In the system status module, a timer widget was set to write the system parameters and monitoring data to a text file for a short period (10 s). The data saved in the text file was used to train the ANN. The historical record module was used to show the past control parameters and water quality data changes in the form of a trend line.

To observe the effect of precipitation time, a tee joint was set in the inlet pipeline of the sedimentation tank. The water that came from the flocculation tank flowed into a beaker, and using a syringe without a needle, a water sample was collected 1 cm below the water face in a short time period to measure the water's turbidity. The SS was determined according to the suspended substance-gravimetric water quality determination method of the People's Republic of China National Standard (GB 11901-89).

Back-propagation neural network (BPNN)

BPNN resembles the human brain in that the model learns and stores knowledge (Mehra and Wah 1992). It is composed of an input layer, one or more hidden layers, and an output layer (Fig. 5). The number of input nodes X_i corresponds to the number of experimental control conditions and the number of output nodes Y_n corresponds to the number of monitoring indicators. BPNN is an overall approximation network, designed as a mathematical model that can learn to find a function that best maps a set of inputs to its correct output using the error back propagation algorithm (Hush and Horne 1993; Nazari and Ersoy 1992). During the training of a BPNN model, the weights between the nodes in the different layers are amended to decrease errors between the predicted and authentic values. When the BPNN achieves the required accuracy, the training is complete and the model can be used for predictions with different input data.

General regression neural network (GRNN)

GRNN was developed as an alternative to the radial basis function neural network (Speacht 1991) and is built completely differently from BPNN, which is based on non-linear regression theory. The GRNN consists of four neuron layers:

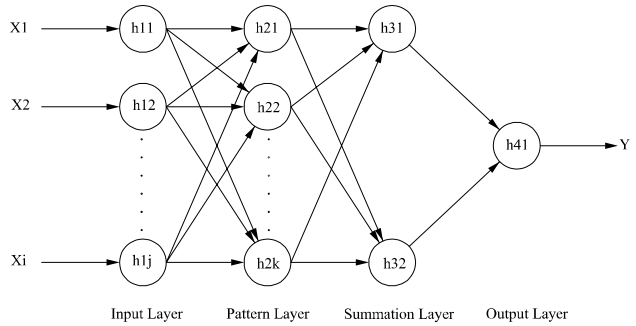

Fig. 6 Typical structure of GRNN

an input layer, a pattern layer, a summation layer, and an output layer (Fig. 6).

In the input layer, the neurons have no transfer function, and the input variables are transferred directly to the pattern layer, in which the number of neurons are equal to the number in the input layer, and every neuron input in the pattern layer corresponds to a different input layer's neurons output by the ergodic method. The Gaussian function was selected as the transfer function of the second layer neuron and the output of every neuron is represented in Eq. (1):

$$\theta_n = \exp\left(-\frac{||X - X_n||^2}{2\sigma^2}\right) \tag{1}$$

where X is the input vector, X_n is the weight vector, $||X - X_n||$ is the Euclidean distance between the vector X and X_n, and σ is the smoothing factor. From Eq. (1), when the input vector X is close to the weight vector X_n, $||X - X_n||$ will be almost 0 and the output θ_n will be close to the maximum value of 1. The smoothing factorσ is used to adjust the neuron's sensitivity to changes in the input.

The third layer is a summation layer, which includes two different types of neurons. One type is used to calculate the arithmetic summation of all the outputs that come from the pattern layer neurons, the transfer function of which is represented in Eq. (2):

$$S_D = \sum_{n=1}^{N} \theta_n \tag{2}$$

The other type is used to calculate the weighted summation of all of the output that comes from the pattern layers. The transfer function is represented in Eq. (3):

$$S_j = \sum_{n=1}^{N} y_{nj}\theta_n \quad (\mathrm{j} = 1, 2, \ldots, \mathrm{J}) \tag{3}$$

where y_{nj} are the weights. The fourth layer is the output layer. The numbers of neurons are equal to the dimension Y of the output vector. The neurons divide the output of the summation layer; the output layer neurons' transfer function is represented in Eq. (4):

$$\hat{y}_j = \frac{S_j}{S_D} = \frac{\sum_{n=1}^{N} y_{nj} \exp\left(-\frac{||X-X_n||^2}{2\sigma^2}\right)}{\sum_{n=1}^{N} \exp\left(-\frac{||X-X_n||^2}{2\sigma^2}\right)} \tag{4}$$

The ANN performance was measured by R^2 and RMSE between the predicted and authentic values, as calculated by Eqs. (5) and (6), respectively (Pendashteh et al. 2011).

$$R^2 = 1 - \frac{\sum_{i=1}^{n}\left(y_i^* - y_P^{(i)}\right)^2}{\sum_{i=1}^{n}\left(y_i^* - \overline{y}\right)^2} \tag{5}$$

$$RMSE = \sqrt{\frac{1}{n}\sum_{i=1}^{n}\left(y_P^{(i)} - y_i^*\right)^2} \tag{6}$$

where $\overline{y}$ is the average of y over the n data, and y_i^* and $y_P^{(i)}$ are the ith target and predicted responses, respectively.

Results and discussion

Selection of the optimum coagulant/flocculent and determination of the best dosage

As described by the classical coagulation mechanism, as the coagulant dosage was increased, the TRRs and SRRs of different coagulants were all in the increasing-stable-decreasing tendency. The results (Supplemental Fig. 1) showed that the PAC achieved higher TRR and SRR at the lower dosage. The better performance of the PAC was because it is a kind of inorganic polymer coagulation, which means that under the combined action of electrical neutralization and adsorption bridging mechanisms, the SS in water are more easily removed. Given the market price of the three coagulants, PAC was the optimum coagulant, and the best dosage was 100 mg/L.

The synergistic reaction of coagulant and flocculent made the TRRs and SRRs of the three PAMs all relativity high and stable. The results (Supplemental Fig. 2) showed that the different electrical properties of the PAM had little influence on TRR and SRR. Meanwhile, considering the different price of the three PAMs, the anion-PAM was the best flocculent, and the best dosage was 4 mg/L.

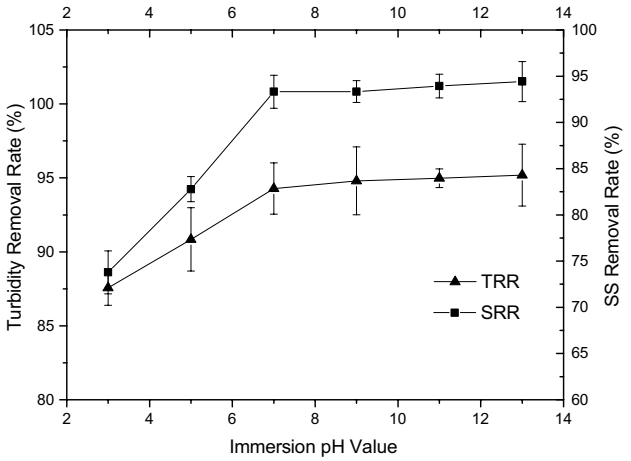

Fig. 7 TRR and SRR of different immersion pH, coagulation tank stirring intensity 200 r/min, mixed tank stirring intensity 200 r/min, flocculation tank stirring intensity 100 r/min, PAC dosage 100 mg/L, flocculant dosage 4 mg/L, magnetic seed 0 mg/L, settling time 120 s

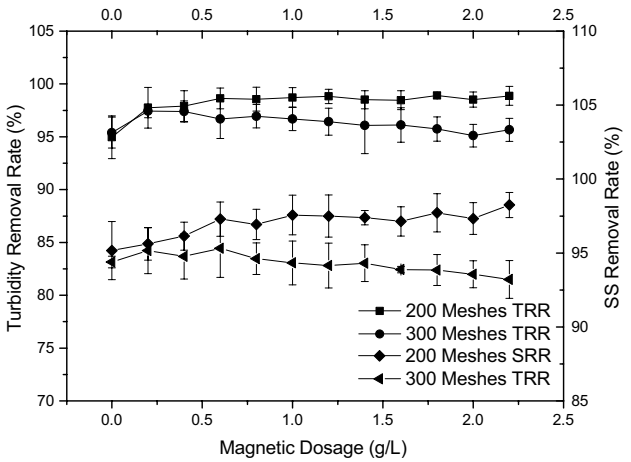

Fig. 8 TRR and SRR of different magnetic seed, pH 7.2, coagulation tank stirring intensity 200 r/min, mixed tank stirring intensity 200 r/min, flocculation tank stirring intensity 100 r/min, PAC dosage 100 mg/L, flocculant dosage 4 mg/L, settling time 120 s

Selection of optimum immersion pH for magnetic seed

To activate the functional groups on the surface of the magnetic seed, it is necessary to immerse the magnetic seed in an alkaline solution (pH = 11) for 24 h (Pavlova and Dobrevsky 2005). Figure 7 presents the relationships between the immersion pH, TRR, and SRR. When the immersion pH was increased from less than 7, both TRR and SRR improved rapidly, but increasing the immersion pH further did not significantly improve TRR and SRR. The results also showed that an alkaline environment helped the tiny flocs to attach to the magnetic seeds in the water.

Selection of the optimum magnetic seed mesh and determination of the best dosage

The relationship curves between the magnetic seed dosage and the TRR and SRR are presented in Fig. 8. According to Fig. 8, when 200-mesh magnetic seed was injected, as the dosage increased, both TRR and SRR increased. Compared with the 200-mesh magnetic seed, the TRR and SRR curves of the 300-mesh magnetic seed had a reverse tendency. In summary, the best size of the magnetic seed was 200-mesh, and the best dosage was 1 g/L. According to a comprehensive analysis of the coagulant/flocculent experimental results and Fig. 8, as the coagulant dosage increased, the TRR had a 42% increment and the SRR had a 13% increment. With the best coagulant and dosage, as the flocculant was increased, the TRR and the SRR were respectively improved by 21 and 22%. However, compared with the control situations with constant dosages of both the coagulant and flocculent, the optimum magnetic seed and best dosage had no significant effect on the TRR and SRR; the TRR only improved by 4%, and the SRR had only a 3% increment. This implies that in the process of removing SS from the coal mine water, the dosage of the magnetic seed contributed little to TRR and SRR.

Selection of the optimum stirring intensity

Stirring intensity influences floc generation. The relationships between the different stirring intensity in the coagulation, mixing, and flocculation tanks and the TRR and SRR are presented in Fig. 9. As the figure shows, the stirring intensity in the three tanks should be reduced step by step with the coal mine water flow. The optimum stirring intensities were 300 r/min for the coagulation tank, 200 r/min for the mixing tank, and 100 r/min for the flocculation tank.

Selection of the optimum precipitation time

With increased precipitation time, the TRRs all increased, with or without magnetic seed (Fig. 10). However, with magnetic seed, the TRR reached 95% in a relatively short time (15 s), and stayed stable for a longer time. This means that the dosage of the magnetic seed significantly increased the floc precipitation speed and allowed the outlet TRR to stabilize very quickly. This means that the sedimentation tank will have a higher surface loading rate (i.e. better precipitation performance).

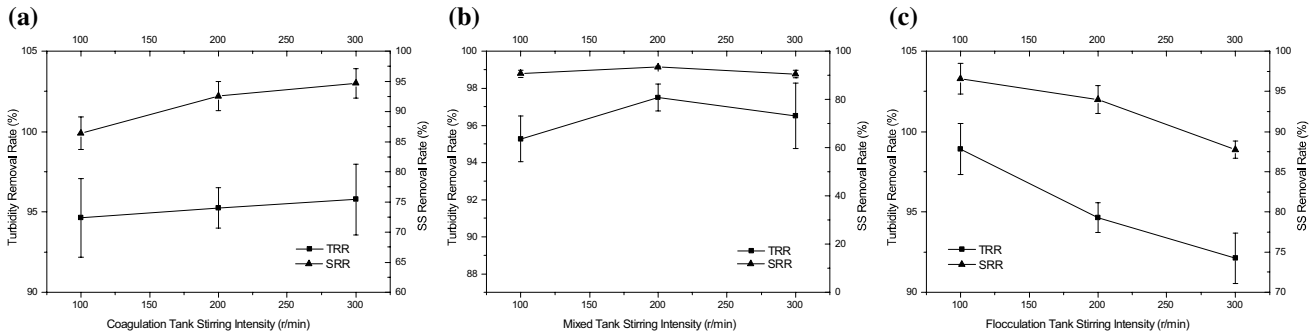

Fig. 9 TRR and SRR of different stirring intensity (**a**) in the coagulation tank, pH 7.5, mixed tank stirring intensity 200 r/min, flocculation tank stirring intensity 100 r/min (**b**) in the mixed tank, pH 7.5, coagulation tank stirring intensity 300 r/min, flocculation tank stirring intensity 100 r/min (**c**) in the flocculation tank, pH 7.4, coagulation tank stirring intensity 300 r/min, mixed tank stirring intensity 200 r/min. PAC dosage 100 mg/L, flocculant dosage 4 mg/L, 200-mesh magnetic seed 1 g/L, settling time 120 s

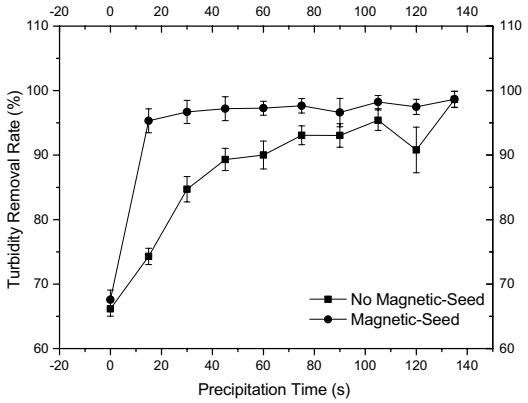

Fig. 10 TRR of different precipitation time with or without magnetic seed, pH 7.7, coagulation tank stirring intensity 300 r/min, mixed tank stirring intensity 200 r/min, flocculation tank stirring intensity 100 r/min, PAC dosage 100 mg/L, flocculant dosage 4 mg/L

Acquisition of artificial neural network (ANN) training data

From the above experimental results, certain levels could be determined; the PAC was 100 mg/L; the anionic PAM was 4 mg/L; the 200-mesh magnetic seed was 1 g/L; the optimum stirring intensity for the coagulation tank was 300 r/min; for the mixing tank was 200 r/min; and for the flocculation tank was 100 r/min. The process of training an ANN needs repeated iterations, so the amount of data used to train the network will directly affect the regression accuracy of the neural network. It is necessary to expand the parameters that influence the TRR of the outlet to obtain more mapping relationships between reaction conditions and results to train the ANN. Thus, the optimum experimental conditions obtained above were selected as the certain levels and expanded to upper and lower levels around the certain level. A total of 3^6 = 729 different kinds of reaction conditions were generated; some reaction condition samples are presented in Table 2. All of the reaction condition items were saved in a text file, which was imported into the MFICS. The MFICS would read the items in the text one by one and adjust the corresponding actuating mechanism automatically. The inlet and outlet turbidity was measured by a turbidity meter, and the turbidity data was automatically recorded by the MFICS. Ultimately, 729 items of recording data were obtained and 700 items of record data were selected to train the network in a random method; the last 29 groups were used to verify the network's regression ability.

Determination of basic parameters of bp neural network (BPNN)

Before the BPNN is trained, certain parameters had to be determined and initialized. The diverse parameters that are initialized with different values will affect the forecast accuracy of the results. In this experiment, the iteration number of BPNN was 200; the gradient correction method was selected as the learning algorithm to modify the weights and thresholds between the neurons; the learning rate was 0.1; the convergence error in the network training process was 0.0004; the input layer nodes were 6 and the output layer node was 1, as detailed in Table 2. Due to the complex mapping relationship between the reaction conditions and the TRR, the number of the hidden layer was 2 and the number of nodes for each hidden layer was 15, which means the network structure was 6-15-15-1.

Of the variety of choices for the node transfer function (NTF) of the BPNN, the NTFs usually utilized are logsig(), tansig(), and purelin(). Their formulas are presented in Eqs. (7)–(9).

Table 2 Some reaction condition samples

Sorting	PAC dosage/(mg/L)	PAM dosage/(mg/L)	200 meshes sand/(g/L)	Coagulation tank stirring intensity/(r/min)	Mixed tank stirring intensity/(r/min)	Flocculation tank stirring intensity /(r/min)	TRR/(%)
1	40	2	0.4	200	100	50	82
2	60	2	0.4	200	100	50	88
3	80	2	0.4	200	100	50	90
4	40	4	0.4	200	100	50	90
5	60	4	0.4	200	100	50	91
6	80	4	0.4	200	100	50	93
…	…	…	…	…	…	…	…
724	40	4	0.8	400	300	150	88
725	60	4	0.8	400	300	150	89
726	80	4	0.8	400	300	150	91
727	40	6	0.8	400	300	150	94
728	60	6	0.8	400	300	150	95
729	80	6	0.8	400	300	150	98

PAC polyaluminium chloride, *PAM* polyacrylamide, *TRR* turbidity removal rate

1) logsig() function:

$$y = 1/[1 + \exp(-x)] \tag{7}$$

2) tansig() function:

$$y = 2/[1 + \exp(-2x)] - 1 \tag{8}$$

3) purelin() function:

$$y = x \tag{9}$$

During initialization, the tansig() function was selected as the hidden layer NTF, and the purelin() function was selected as the output layer NTF.

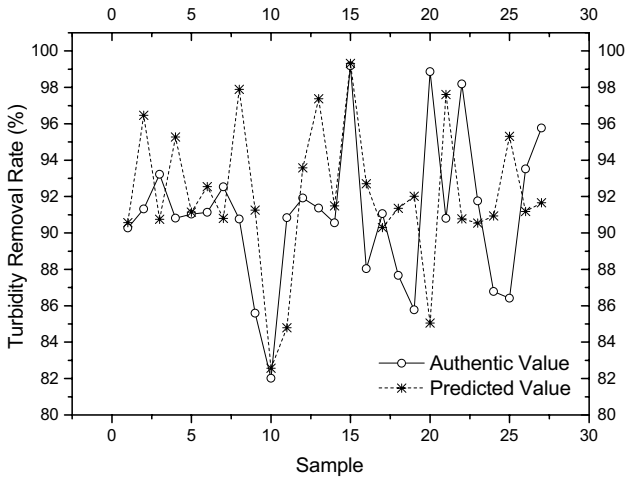

Fig. 11 Comparison between the authentic values and predicted values of BPNN

Predicted results of the BPNN and parameter adjustment

Only three predicted value figure points were in the circles of the authentic value, and it was difficult for BPNN to determine the regression relation between the predicted and authentic value (Fig. 11). The error distribution is presented in Fig. 12. The numbers in the tolerance scope of less than 3% were 12; the numbers in the tolerance scope between 3 and 6% were 7; the numbers in the tolerance scope between 6 and 9% were 7; the number in the tolerance scope between 9 and 12% was 0; the number in the tolerance scope between 12 and 15% was 1. Thus, all data errors were less than 15%; the R^2 was 0.2970 and the RMSE was 4.1087.

Predictive errors with different NTFs are presented in Table 3. According to Table 3, the R^2 was maximized and the RMSE was the smallest when the purelin() function was selected as the hidden layer NTF and the logsig() function was selected as the output layer NTF. The predicted and actual values of the BPNN for the optimal NTF are presented in Fig. 13. Compared with Fig. 11, the predicted BPNN values that set the optimal NTF better matched the actual values.

In determining the basic parameters of the BPNN section, a multi-hidden layer neural network was selected for fitting the relationship of the six inputs and one output. The different numbers of hidden layer nodes and their R^2 and RMSE are presented in Table 4. If the items are grouped by the node number of the 1st hidden layer, when the node number of the 2nd hidden layer was 20 in every group, the R^2 always would be the maximum and the RMSE would be the minimum. If the items are grouped by the node number of

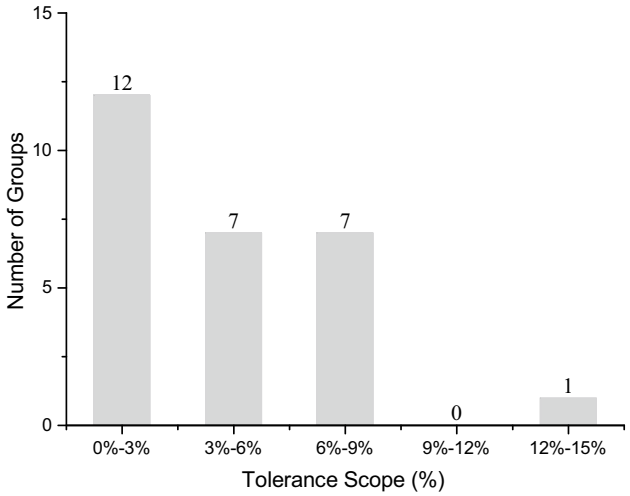

Fig. 12 Error distribution of BPNN results

Table 3 Effects of different NTF on R^2 and RMSE

Hidden layer function	Output layer function	R^2	RMSE
Logsig	Tansig	−0.0746	6.0659
Logsig	Purelin	0.2283	3.4450
Logsig	Logsig	0.2116	5.4822
Tansig	Tansig	0.1210	3.6767
Tansig	Logsig	0.1405	4.6358
Tansig	Purelin	0.2734	3.3428
Purelin	Logsig	0.5203	2.0928
Purelin	Tansig	0.0692	3.7835
Purelin	Purelin	0.3327	3.2036

NTF node transfer function, R^2 R-squared, *RMSE* root-mean-square error

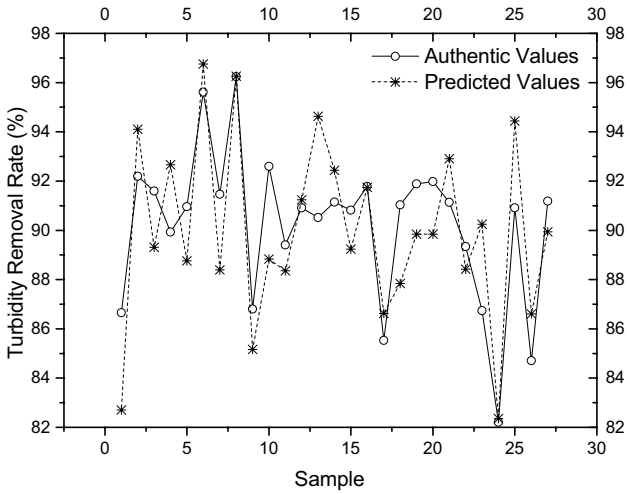

Fig. 13 Comparison between the authentic values and predicted values of BPNN in best NTF

Table 4 Effects of different hidden layer nodes on R^2 and RMSE

1st hidden layer nodes number	2nd hidden layer nodes number	R^2	RMSE
10	10	0.2217	2.6657
10	20	0.5336	2.0636
10	30	0.5130	2.1086
20	10	0.2751	2.5726
20	20	0.8583	1.1373
20	30	0.5529	2.0204
30	10	0.6653	1.7481
30	20	0.7347	1.6951
30	30	0.6472	1.7943

R^2 R-squared, *RMSE* root-mean-square error

the 2nd hidden layer, when the node number of the 1st was altered, no significant change in the regular pattern could be found. When the node numbers of both hidden layers were 20 for all items, the R^2 was the highest, and the RMSE was the lowest. The highest R^2 was 0.8583 and the lowest RMSE was 1.1373. In summary, for a multi-hidden layer BPNN, the best network structure was 6-20-20-1, the best hidden layer NTF was the purelin function, the best output layer NTF was the logsig function, and the highest R^2 that the BPNN could reach was 0.8583.

Determination of GRNN Parameters

Compared with the BPNN, GRNN has no need to adjust the connection weight between neurons. The primary advantage of GRNN is in the process of network training. To achieve better regression capacity, there is only one parameter, the smoothing factor, that has to be adjusted. To determine the smoothing factor easily, Sprecht (1991, 1993) proposed an effective four-step method: (1) the span(F_{min}, F_{max}) and the step length $\Delta\alpha$ of the smoothing factor increase are determined; (2) samples are randomly selected to train the network with the smoothing factor calculated from the previous step, and the remaining samples are utilized to verify the trained network; (3) the error sequence between the predicted values and the authentic values are recorded, and the R^2 and RMSE value of the error sequence are used as the index to evaluate the regression capacity of the neural network; and (4) the smoothing factor that corresponds to the maximum of R^2 and minimum of RMSE can be used as the GRNN parameter.

Performance and analysis of the GRNN

The regression results of GRNN are presented in Fig. 14. Compared with Fig. 13, the TRR gaps between the authentic

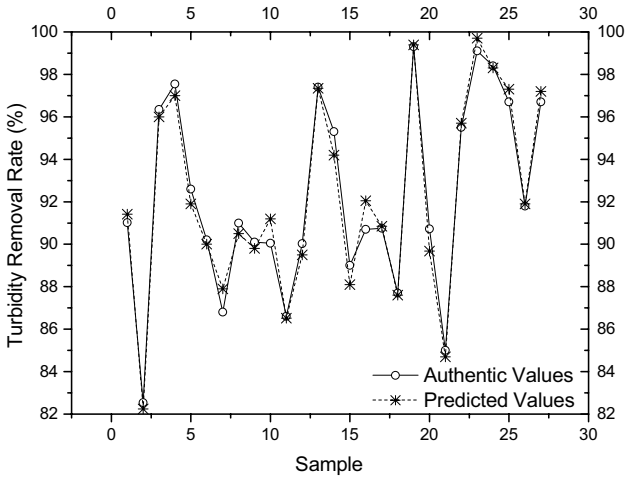

Fig. 14 Comparison between the authentic values and predicted values of GRNN

Table 5 BPNN and GRNN neural network predicted results

Index	BPNN		GRNN	
	Training values	Test values	Training values	Test values
R^2	0.8762	0.8583	0.9894	0.9801
RMSE	0.9746	1.1373	0.3983	0.4392

R^2 R-squared, *RMSE* root-mean-square error, *BPNN* back propagation neural network, *GRNN* generalized regression neural network

values and the predicted values were smaller. The R^2 of GRNN was 0.9801, and the RMSE was 0.4392. The optimal smoothing factor was 0.5843.

Comparison and analysis of the regression ability of BPNN and GRNN

The optimum parameters obtained above were used to compare the regression ability of BPNN and GRNN. From Table 5, for both the training and the test values, GRNN had the higher R^2 and lower RMSE, which means that GRNN was better able to regress to the relationships between the reaction conditions and the monitor indexes. Therefore, GRNN had better predictability for magnetic-flocculation treatment of mine water and was more suitable for apparatus control.

Conclusions

In this study, the coagulant and flocculant dosages, magnetic seed immersion pH, stirring intensity, and precipitation time were all selected as inspection conditions to determine the optimum reaction conditions. Based on a comprehensive consideration of the results and economic costs, the PAC and anionic PAM were the best coagulant and flocculant for this application. A neutral and alkaline environment was beneficial to magnetic flocculation, but a higher pH gave no significant improvement. While optimizing the size and the dosage of the magnetic seed contributed little to TRR and SRR, the magnetic seed dosage did increase the floc precipitation speed, which means that the sedimentation tank can have a higher surface loading rate. In the coagulation, mixing, and flocculation tanks, the stirring intensity should be reduced step by step with the growth of the flocs.

BPNN and GRNN were used to regress the relationship between the reaction conditions and the monitoring index. Compared with the GRNN, BPNN had more parameters that needed adjustment. To achieve a better regression ability, the BPNN had to modify the learning algorithm, learning rate, convergence error, and the network structure, which make the engineering application more difficult and reduces efficiency. GRNN had only one parameter, the smoothing factor, that had to be adjusted to match the reaction process, and thus is better for precisely controlling an engineering application.

Acknowledgements This work was supported by the Natural Science Foundation of Hebei Province (Grant 15274006D).

References

Almeida JS (2002) Predictive non-linear modeling of complex data by artificial neural networks. Curr Opin Biotech 13(1):72–76

Gao L, Connor J, Doble R, Ali R, McFarlane D (2013) Opportunity for peri-urban Perth groundwater trade. J Hydrol 496:89–99

Guclu D, Dursun S (2010) Artificial neural network modelling of a large-scale wastewater treatment plant operation. Bioprocess Biosyst Eng 33(9):1051–1058

Hong SH, Lee MW, Lee DS (2007) Monitoring of sequencing batch reactor for nitrogen and phosphorus removal using neural networks. Biochem Eng J 35(3):365–370

Hush D, Horne B (1993) Progress in supervised neural networks. IEEE Signal Proc Mag 10(1):8–39

Kirby M, Connor JD, Ahmad M, Gao L, Mainuddin M (2014) Climate change and environmental water reallocation in the Murraye-Darling Basin: impacts on flows, diversions and economic returns to irrigation. J Hydrol 518(2):120–129

Kirby M, Connor JD, Ahmad M, Gao L, Mainuddin M (2015) Irrigator and environmental water management adaptation to climate change and water reallocation in the Murraye-Darling Basin. Water Econ Policy 01(03):155–199

Li YR, Wang J, Zhao Y, Luan ZK (2010) Research on magnetic seeding flocculation for arsenic removal by superconducting magnetic separation. Sep Purif Technol 73(2):264–270

Mehra P, Wah BW (1992) Artificial neural networks. In: Wah BW (ed) Artificial neural networks: concepts and theory, 1st edn. IEEE Computer Society Press, Los Alamitos, pp 1–12

Nazari J, Ersoy O (1992) ECE technical reports. School of Electrical Engineering Purdue University, Indiana, USA. https://docs.lib.purdue.edu/cgi/viewcontent.cgi?article=1279&context=ecetr

Pavlova S, Dobrevsky I (2005) Modified Sirofloc process for natural water treatment. Desalination 173(1):55–59

Pendashteh A, Fakhru'l-Razi A, Chaibakhsh N, Abdullah LC, Madaeni SS, Abidin ZZ (2011) Modeling of membrane bioreactor treating hypersaline oily wastewater by artificial neural network. J Hazard Mater 192(2):568–575

Speacht DF (1991) A general regression neural networks. IEEE T Neural Networ 2(6):568–576

Sprecht DF (1993) The general regression neural network-rediscovered. Neural Networks 6(7):1033–1034

Tsouris C, Scott TC (1995) Flocculation of paramagnetic particles in a magnetic field. J Colloid Interf Sci 171(2):319–330

Wang WP, Gao L, Liu P, Hailu A (2014) Relationships between regional economic sectors and water use in a water-scarce area in China: a quantitative analysis. J Hydrol 515(13):180–190

Yiacoumi S, Rountree DA, Tsouris C (1996) Mechanism of particle flocculation by magnetic seeding. J Colloid Interf Sci 184(2):477–488

Zhao Y, Liang WY, Liu LJ, Li FZ, Fan QL, Sun XL (2015) Harvesting *Chlorella vulgaris* by magnetic flocculation using Fe_3O_4 coating with polyaluminium chloride and polyacrylamide. Bioresource Technol 198:789–796